The β3-integrin endothelial adhesome regulates microtubule dependent cell migration.

Samuel J Atkinson[1], Aleksander M Gontarczyk[1], Abdullah AA Alghamdi[1], Tim S Ellison[1], Robert T Johnson[1], Wesley J Fowler[1], Benjamin M Kirkup[1], Bernardo C Silva[1], Bronwen E Harry[1], Jochen G Schneider[2], Katherine N Weilbaecher[3], Mette M Mogensen[1], Mark D Bass[4], Maddy Parsons[5], Dylan R Edwards[6] and Stephen D Robinson[1]*.

Affiliations:

[1]School of Biological Sciences, University of East Anglia, Norwich Research Park, Norwich, UK.

[2]Luxembourg Center for Systems Biomedicine (LCSB), University of Luxembourg, Luxembourg & Saarland University Medical Center, Internal Medicine II, Homburg, Germany, Centre Hospitalier Emily Mayrisch, Esch, Luxembourg.

[3]Department of Internal Medicine, Division of Molecular Oncology, Washington University in St Louis, St. Louis, MO, USA.

[4]Centre for Membrane Interactions and Dynamics, Department of Biomedical Science, University of Sheffield, Sheffield, UK.

[5]Randall Division of Cell and Molecular Biophysics, King's College London, New Hunt's House, Guys Campus, London, UK

[6]Faculty of Medicine and Health Sciences, University of East Anglia, Norwich Research Park, Norwich, UK.

Running title: The β3-integrin endothelial adhesome

Key words: adhesome, endothelial, integrins, microtubules

*Corresponding author

Integrin β3 is seen as a key anti-angiogenic target for cancer treatment due to its expression on neovasculature, but the role it plays in the process is complex; whether it is pro- or anti-angiogenic depends on the context in which it is expressed. To understand precisely β3's role in regulating integrin adhesion complexes in endothelial cells, we characterised, by mass spectrometry, the β3-dependent adhesome. We show that depletion of β3-integrin in this cell type leads to changes in microtubule behaviour that control cell migration. β3-integrin regulates microtubule stability in endothelial cells through Rcc2/Anxa2 driven control of active Rac1 localisation. Our findings reveal that angiogenic processes, both *in vitro* and *in vivo*, are more sensitive to microtubule targeting agents when β3-integrin levels are reduced.

Introduction

Angiogenesis, the formation of new blood vessels from those that already exist, plays an essential role in tumour growth [1]. As such, targeting angiogenesis is seen as crucial in many anti-cancer strategies [2]. Therapies directed against vascular endothelial growth factor (VEGF) and its major receptor, VEGF-receptor-2 (VEGFR2), whilst effective in a number of cancers, are not without side-effects due to the role this signaling pathway plays in vascular homeostasis [3]. Fibronectin (FN)-binding endothelial integrins, especially αvβ3- and α5β1-integrins, have emerged as alternative anti-angiogenic targets because of their expression in neovasculature [4, 5]. However, neither global nor conditional knockouts of these integrins block tumour angiogenesis long-term [6-8], and clinical trials of blocking antibodies and peptides directed against these extracellular matrix (ECM) receptors have been disappointing [9, 10]. To gain novel insight into how αvβ3-integrin regulates outside-in signal transmission [11], we have undertaken an unbiased analysis of the molecular composition of the mature endothelial adhesome, and profiled changes that occur when β3-integrin expression is manipulated. In so doing, we have uncovered β3-integrin dependent changes in microtubule behaviour that regulate cell migration.

Results and Discussion

The isolation and analysis of integrin adhesion complexes (IACs) by mass-spectrometry (MS) is difficult because of the low affinity and transient nature of the molecular interactions occurring at these sites. However, using cell-permeant chemical crosslinkers improves recovery of IAC proteins bound to either FN-coated microbeads [12] or plastic dishes [13]. These advances have led to the characterisation of IACs from a number of cell types. Whilst a core consensus adhesome (the network of structural and signaling proteins involved in regulating cell-matrix adhesion [14]) can be defined [12], the composition and stoichiometry of the meta-adhesome depends on the cell-type being analysed, the integrin-receptor repertoire expressed by that cell type, and on any imposed experimental conditions. To examine the composition of the endothelial adhesome we isolated lung microvascular endothelial cells (ECs) from C57BL6/129Sv mixed background mice and immortalised them with polyoma-middle-T-antigen by retroviral transduction [15]. As our main interest was in establishing how β3-integrin influences the endothelial adhesome, we adhered cells to FN for 90 minutes, which allows β3-rich (mature) focal adhesions (FAs) to form [16]. To distinguish integrin-mediated recruitment of proteins from non-specific background, we also plated cells on poly-L-lysine (PLL) as a negative control (adhesion to PLL does not depend on integrins). Visualisation of neuropilin-1 staining in whole cells showed that this protein, which we previously demonstrated is present in the mature EC adhesome [17], co-localises with talin-1 in FAs when cells are plated on FN, but not PLL (Fig. 1A). For all proteomics experiments, we crosslinked FAs using the cell permeant and reversible cross-linkers DPDPB and DSP (see materials and methods) for 5 minutes. Cells were lysed and subjected to a high sheer flow water wash to remove non-crosslinked material. Crosslinking was reversed, and samples were precipitated and concentrated for analyses. Prior to MS, samples were quality controlled by SDS/PAGE and silver-staining to ensure efficient removal of non-crosslinked material had occurred (Fig. 1B).

Label-free proteomic analyses of the FN + VEGF, FN, and PLL adhesomes (Fig. 1C; Table EV1) initially detected and quantified 1468 proteins. Stringent filtering, requiring proteins to be detected in all 3 repeats of at least one condition, left 1064 proteins – a high confidence dataset that was used to define the endothelial adhesome. Hierarchical clustering based on average Euclidian distance identified 12 clusters (A-L) which could be considered VEGF-enriched proteins (A-C), FN-enriched (D-F), and PLL-enriched (G-L). Fisher's exact test enrichment analysis was carried out to identify which pathway, process, or component proteins within these clusters belong to using Gene Ontology annotations. Cell projection (GOCC, $p=8.62 \times 10^{-5}$) and microtubule (GOCC, $p=1.6 \times 10^{-4}$) categories were significantly enriched when cells were treated with growth factor, suggesting they are important in VEGF-mediated processes. Leukocyte trans-endothelial migration (KEGG, $p=9.71 \times 10^{-5}$) proteins were enriched in the FN adhesome, but not in the VEGF-stimulated adhesome, suggesting our cells represent quiescent vasculature without VEGF-stimulation. This same category contains many endothelial specific proteins (e.g. VE-cadherin, Cdh5), further confirming that the cells have an endothelial identity. Focal adhesion (KEGG, p=9.31x10^{-7}) proteins were enriched in the FN adhesome but depleted in the PLL adhesome, confirming the success of the adhesome enrichment process, MS, and downstream analysis. Other adhesion/migration associated categories: focal adhesion (GOCC, p=5.99 x 10^{-5}), cell projection (GOCC, p=3.03 x 10^{-5}), cell adhesion (GOBP, p=1.61 x 10^{-6}) and lamellipodium (GOCC, p=1.38 x 10^{-4}) were depleted in the PLL adhesome.

To test the consequences of excluding β3-integrin from the EC adhesome, we decided to profile changes in β3-heterozygous (β3HET) ECs, which carry one wild-type allele of β3-integrin, and one knockout allele. These cells express 50% wild-type levels of β3-integrin. As in previous studies, we decided to use β3HET cells for these initial analyses, rather than β3-integrin knockout (β3NULL) cells, hypothesising this would circumvent potential developmental changes arising from the complete loss of the protein, which we felt might confound quantitative interpretations of the EC adhesome; we have shown these cells are a good model for studying the role of αvβ3-integrin in cell migration, whilst evading changes arising from the complete loss of the integrin on both alleles (e.g. up-regulated total VEGFR2 expression) [17]. Both wild-type (β3WT) and β3HET ECs adhere equally to saturating concentrations (10 μg/ml) of FN (see Ellison *et al*., 2015 [17]). To compare the size distribution of FAs between β3WT and β3HET ECs (which might affect the stoichiometry of components in the adhesome), we seeded cells for 90 minutes on FN, immunostained for paxillin, and measured FA area; we noted no differences in the percentage of FA size distributions between the two genotypes (Fig. 2A). Therefore, MS analyses comparing the adhesome between β3WT and β3HET ECs were performed (Fig. 2B; Table EV2). Enrichment analysis showed a depletion of cytoskeletal components (GOCC, p = 4.73 x 10^{-5}) in the β3WT adhesome when compared with the β3HET adhesome, despite the enrichment of adhesion/migration associated categories previously noted in the FN adhesome of β3WT ECs (Fig. 1C). Whilst a majority of individual FA components in the mature adhesome do not change upon β3-integrin depletion, downstream connections to cytoskeletal components do. We took a particular interest in microtubules (MTs) because by SAM analysis all detected tubulins were significantly upregulated in the β3HET adhesome. To confirm this finding by other means, we probed western blots for α-tubulin and showed a significant increase in FA-enriched samples from β3HET cells compared with β3WT cells (Fig. 2C).

Our findings intimated that αvβ3-integrin drives MT localisation away from FAs. To increase the power of our downstream mechanistic analyses, we felt it appropriate to now also include β3NULL ECs in our studies. We examined MT organisation in β3WT, β3HET, and β3NULL ECs by immunolabeling for α-tubulin in whole cells (Fig. 3A). No gross changes in cell microtubule arrays were observed. Furthermore, total cellular levels of α-tubulin were similar across all three genotypes (Fig. 3B). However, co-localisation of MTs at peripheral FAs was greater in β3HET and β3NULL ECs, compared to β3WT ECs, as was extension into lamellipodea (Fig. 3C; for an example of quantification of the latter, see Fig. EV1). Overall, the findings suggest that β3-integrin limits the targeting of MTs to FAs.

Given that MTs can drive FA turnover, and thus cell migration [18], we next tested whether EC migration is differentially sensitive to microtubule targeting agents (MTAs) in β3HET and β3NULL ECs. For each MTA examined, we first determined the dose of the compound that allowed 90 percent survival of β3WT ECs (see materials and methods), and then tested the effects of this dose on random migration in β3WT, β3HET, and β3NULL cells (Fig. 3D; raw migration data shown in Fig. EV2). Random migration was affected by MT stabilisers (Paclitaxel, Epothilone B) in cells of all three genotypes, However, β3WT ECs were insensitive to the MT destabilisers tested (Colchicine, Mebendazole, Fosbretabulin) and the mechanistically unique MTA Eribulin (which functions through an end poisoning mechanism [19]), whilst β3HET and β3NULL ECs generally showed a sensitivity to all classes of compounds tested. We extended these types of analyses *in vivo* to examine the effects of Eribulin and Fosbretabulin on tumour growth and angiogenesis. We chose these two MTAs as they are well tolerated in mice [20, 21] and used clinically in humans. We settled on suboptimal doses (see materials and methods) that would allow us to observe potential synergy with endothelial depletion of β3-integrin. β3-integrin-floxed/floxed mice [22] were bred with Tie1Cre mice [23] to generate β3-integrin-floxed/floxed Cre-positive animals (Cre-negative littermates were used as controls). CMT19T lung carcinoma cells were injected subcutaneously and allowed to establish for 7 days, at which point the MTAs were administered (see materials and methods for dosing regimes). Neither Eribulin nor Frosbretabulin had any effect on tumour growth in Cre-negative animals compared with vehicle treated animals, but tumour growth was reduced in MTA-treated Cre-positive animals (Fig. 3E). Analysis of tumours by immunostaining for blood vessels showed a reduction in intratumoral microvascular density only in sections from MTA-treated Cre-positive animals (Fig. 3F). These studies suggested that the loss of endothelial β3-integrin sensitises angiogenic responses to MT destabilisers both *in vitro*, and *in vivo*.

The increased sensitivity to destabilising MTAs suggested to us that there is an increased population of stable MTs in β3HET and β3NULL ECs compared with their wild-type counterparts. We explored this premise by exposing ECs to cold temperatures (which destabilises MTs), washing out tubulin monomers [24], followed by immunolabelling for α-tubulin. We noted elevated stable MTs in both β3HET and β3NULL cells (Fig. 4A). Re-introducing β3-integrin into β3NULL cells restored MT sensitivity to cold; MTs were more sensitive to cold treatment in NULL cells expressing full-length human β3-integrin, than MTs in cells transfected with an empty vector control (Fig. EV3). We also measured MT stability biochemically by extracting both cold-sensitive and cold-stable MTs from the same sample of cold-treated cells and western blotting for α-tubulin (Fig. 4B). On whole, β3HET and β3NULL ECs showed decreased cold-sensitive and increased cold-stable MTs compared with β3WT ECs.

To gain further mechanistic insight into how β3-integrin at FAs might be regulating MT function, we delved deeper into our β3-dependent adhesome data. We noted that Rcc2 clusters with β3-integrin in the β3WT adhesome, but is significantly decreased in that of β3HET ECs. Rcc2 (also known as telophase disk protein of 60 kDa, TD-60) has previously been shown to associate with integrin complexes [25] and to regulate MTs [26]. We therefore examined whether Rcc2 was regulating MT stability in ECs. Knocking down Rcc2 by siRNA in β3WT ECs elicited a significant increase in cold-stable MTs (Fig. 5A; see Fig. EV4 for representative MT staining). This finding suggested to us that Rcc2 plays a β3-dependent role in regulating MTs in ECs, but does not do so in isolation. We therefore cross-referenced our adhesome data with an Rcc2 pull-down assay performed from HEK-293T cells (Table EV3) [27]. Some obvious potential candidates (e.g. Coronin-1C) were present in both the β3WT and β3HET adhesomes, but at the same level, so were ruled out from further analysis. However, annexin-a2 (Anxa2) co-precipitates with Rcc2 in HEK-293T cells and, like Rcc2, was reduced in the β3HET adhesome. Therefore, we examined whether Anxa2 was also regulating MT stability in ECs via siRNA-mediated knockdown. Like Rcc2 knockdown, even a relatively small (~30%) Anxa2 knockdown in β3WT ECs elicited a significant increase in cold-stable MTs (Fig. 5B; see Fig. EV4 for representative MT staining). Moreover, a double knockdown of both targets led to an additive increase in cold-stable MTs in β3WT ECs (Fig. EV4).

Both Rcc2 [25, 27] and Anxa2 [28] have been identified as regulators of Rac1, and work by a number of groups has demonstrated that cortical Rac1 activity promotes MT stability [29-31]. Because total Rac1 stoichiometry was unchanged when comparing β3WT and β3HET EC adhesomes, we hypothesised that Rcc2/Anxa2-dependent alterations in Rac1 activity were responsible for altered MT stability in β3HET and β3NULL ECs. First, we tested the premise that Rac1 plays a differential role in regulating MT stability in β3WT and β3-depleted ECs by testing the effects of the Rac1 inhibitor NSC23766. NSC23766 had no effect on MT stability in β3WT cells, but the number of cold stable MTs in both β3HET and β3NULL ECs was reduced in the presence of the inhibitor (Fig. 5C; see Fig. EV4 for representative MT staining). We also demonstrated that the increases observed in MT stability upon Rcc2 or Anxa2 knockdown were abrogated in the presence of NSC23766 (Fig. EV5), suggesting that both proteins regulate MT stability in ECs in a Rac1-dependent manner.

Rcc2 has previously been reported to limit the activation of both Rac1 and Arf6 [25]. Indeed, Rcc2 can guide mesenchymal cell migration by trafficking Rac1 and controlling its exposure to GEFs [27]. We therefore tested whether there were differences in Rcc2/Anxa2/active-Rac1 associations between β3WT and β3-depleted ECs. First, we examined total cellular levels or Rac1 and showed they were equivalent in all three cell lines (Fig. 5D). PAK-PBD pull-downs of GTP-bound Rac1 showed co-association of all three proteins in β3WT, β3HET and β3NULL ECs (Fig. 5E), so we concluded that changes in Rac1 activity alone were not responsible for alterations in MT stability in β3-depleted cells. Humphries *et al.* showed that Rcc2 is recruited to α5β1-FN complexes but not α4β1-Vcam1 (vascular cell adhesion molecule-1) complexes in cells expressing both α4- and α5-integrins [25]. Thus, we also tested associations between Rcc2, Anxa2 and α5-integrin in β3WT and β3-depleted ECs by PAK-PBD pull-downs. Rcc2, Anxa2, β3-integrin and α5-integrin were pulled down with Rac1-GTP in β3WT ECs. Rcc2, Anxa2 were also pulled down with Rac1-GTP in β3HET and β3NULL ECS, whilst β3-integrin-Rac1-GTP associations were lost and α5-integrin-Rac1-GTP associations were increased (Fig. 5E). Given the stoichiometry of α5-integrin in the β3-depleted adhesome is unchanged compared to the β3WT adhesome (Fig. 2) whilst Rcc2 and Anxa2 levels are decreased, we speculated that a substantial proportion of the observed increase in Rcc2/Anxa2/active-Rac1/Itga5 associations in β3-depleted cells occurs away from β3-rich FAs, perhaps in recycling endosomes. Endocytic trafficking of Rac1 is required for the spatial restriction of signaling during mammalian cell migration [32]. In support of this hypothesis, we demonstrated a redistribution of Rac1-GTP in β3-depleted ECs using a Raichu-Rac1 biosensor (Fig.

5F); compared to β3WT ECs, a substantial proportion of active Rac1 in β3HET and β3NULL cells appeared cytoplasmic. This redistribution of active Rac1 appeared to be independent of the total level of active Rac1 present in the cells; active Rac1 levels were only noticeably elevated in β3HET cells (Fig. 5F).

By mining the FN-β3-integrin EC adhesome, not only have we generated a valuable tool for the integrin and angiogenesis communities, we have also utilised the data to uncover a novel role for β3-integrin in regulating MT function/stability during EC migration. We previously showed that endothelial Rac1 is only required for tumour growth and angiogenesis when β3-integrin is absent [33], but the underlying mechanism for this observation has remained unclear. Our working hypothesis is that engagement of αvβ3-integrin with FN at mature FAs localises an Rcc2/Anxa2/Rac1 containing complex to these sites, either preventing GTP-Rac1 from participating in MT stability, or actively destabilising MTs (our experiments do not allow us to distinguish between these two possibilities), perhaps by controlling its exposure to GEFs. When αvβ3 is not present, the complex associates with α5β1-integrin instead, where it now has the opposite effect on MTs (see synopsis). This re-positioning of Rac1 activity means that it plays a role in MT-linked EC migration only when αvβ3 is not present in mature FAs. There is certainly precedence for β3-integrin regulating spatial distribution of signaling pathway components in cells. For example, we previously showed that β3-integrin plays a role in locally suppressing β1-integin in fibroblasts to promote persistent cell protrusion and migration by regulating interactions between vasodilator-stimulated phosphoprotein (Vasp) and Rap1-GTP-interacting adaptor molecule (Apbb1ip/RIAM) [34]. Moreover, MTs have recently been shown to target active β1-integrins [35]. Thus, it will be particularly pertinent to next determine the full composition of the Rcc2/Anxa2/Rac1-GTP complex as many of the proteins that might be suspected to play a role in MT capture (e.g. Clip170 and Clasps) do not appear to be present in the EC adhesome [36]; to gain a full picture of how MT stability/FA targeting are regulated in ECs, it will also be essential to establish how this complex behaves in α5β1-deficient ECs.

Finally, it is worth considering how changes in levels of integrin expression might affect the cellular responses we have examined. Whilst, in general (e.g. sensitivity to MTAs, including cold), β3HET and β3NULL cells behaved similarly in the assays we employed, there are two notable differences: (1) β3NULL cells showed increased MT targeting to lamellipodia, compared to β3HET cells (Fig. 3C), which might suggest altered MT dynamics between the two genotypes. It will be important to examine microtubule dynamics in greater detail (e.g. rates of growth, catastrophe, and rescue) with changes in integrin expression patterns/levels. (2) On fibronectin, β3HET cells showed increased Rac1-GTP levels compared to β3NULL cells (Fig. 5). This might relate to the increased total VEGFR2 levels noted in β3NULL [37] but not β3HET [17] cells. If VEGFR2 is playing a role here, we speculate it is separate from its known interactions with αvβ3-integrin. VEGFR2 and αvβ3-integrin interactions are augmented on vitronectin [38], and we do not detect VEGFR2 in our FN-dependent EC adhesome (Fig. 1). Notwithstanding, our findings suggest that once effective αvβ3-integrin antagonists are available (e.g. ProAgio [39]), they may be particularly useful as anti-angiogenic agents when used in combination with already approved MTAs, such as Eribulin.

Materials and Methods

Reagents

Unless otherwise stated all chemicals used were purchased from Sigma-Aldrich (Poole, UK). Vascular endothelial growth factor (mouse VEGF-A^{164}) was made in house according to Krilleke *et al*. [40].

Animals

All animals were on a mixed C57BL6/129 background. Littermate controls were used for all *in vivo* experiments. All animal experiments were performed in accordance with UK Home Office regulations and the European Legal Framework for the Protection of Animals used for Scientific Purposes (European Directive 86/609/EEC).

Mouse endothelial cell isolation and culture

Mouse lung ECs were isolated from adult mice on a mixed C57BL6/129 background as per Reynolds and Hodivala-dilke [41] then subsequently immortalised and cultured as per Ellison *et al*. [17]. The cell lines used in the studies presented here were cross-referenced to a pure C57BL6 genetic background via a 384 single nucleotide polymorphism panel (Charles River Genetic Testing Services, Wlmington, MA, USA). These analyses showed: β3WT=91.99% C57BL6; β3HET=93.03% C57BL6; β3NULL=44.75% C57BL6.

Adhesion Assay

96 well plates were coated in 10 μg ml^{-1} fibronectin (FN) in phosphate buffered saline (PBS) overnight at 4°C then blocked with 1% bovine serum albumin (BSA) in PBS for 1 hour at room temperature. 20,000 cells were seeded into each well and allowed to

adhere for 90 minutes. Cells were then washed with PBS with 1 mM $MgCl_2$ and 1 mM $CaCl_2$ 3 times to remove non-adherent cells and fixed with 4% paraformaldehyde (PFA) for 10 minutes at room temperature. After a further PBS wash, cells were stained with 1% methylene blue in 10 mM borate buffer pH 8.5/50% Methanol for 30 minutes at room temperature. Excess stain was removed with RO water before a 50% 0.1 M HCl/50% Ethanol destain solution was used for 10 minutes at room temperature. The destain solution was then moved to a new plate and read absorbance was measured at 630 nm.

Focal Adhesion Enrichment

Focal-adhesion enrichment was carried out as described in Ellison *et al*. [17] and Schiller *et al*. [13]. A small amount of each focal adhesion sample generated was quality controlled by running a 10% SDS-PAGE gel followed by silver staining (Pierce ™ Silver Stain Kit, ThermoFisher Scientific, Cramlington, UK). Good quality samples were then analysed by western blotting or mass spectrometry.

Mass Spectrometry (MS)

Mass spectrometry was carried out by the Fingerprints Proteomics Facility (Dundee University, Dundee, UK) as per Schiller *et al*. [13]. Peptides were identified and quantified using MaxQuant [42] software using the Andromeda peptide database. To achieve label-free quantitative results, three biological repeats were pooled and each of these pooled samples was analysed via three technical repeats through the spectrometer.

MS Statistical Analysis

All mass spec analysis was performed using the Perseus [43] bioinformatics toolbox for MaxQuant. Statistical significance was identified using the Significance Analysis of Microarrays (SAM) method [44]. Unsupervised hierarchical clustering was performed using Perseus' built in tools. KEGG and GO annotations were obtained from the mouse annotations package via Perseus (downloaded 20/06/2015) and used to identify angiogenesis, cytoskeleton and focal adhesion related genes.

Random Migration

24 well plates were coated with 10 µg ml^{-1} FN in PBS overnight at 4°C and then blocked with 1% BSA for 1 hour at room temperature. 10,000 ECs were seeded per well and allowed to recover overnight. Media was then replaced with media containing one of the following microtubule targeting agents (MTAs –from Abcam, Abingdon, UK, unless

otherwise noted): Paclitaxel 5nM, Epothilone B 1nM, Colchine 10μM, Mebendazole 0.4μM, Fosbretablin 0.5μM or Eribulin 1μM (a kind gift from Katherine Weilbaecher, Washington University, MO, USA); DMSO was used as a vehicle control. A phase contrast image was taken of each well every 20 minutes using an inverted Axiovert (Zeiss) microscope for 15 hours at 37°C and 5% CO_2. The ImageJ plugin MTrackJ [45] was then used to manually track individual cells and the speed of random migration was calculated.

Microtubule Stability Assays

Microtubule cold stability assays were carried out as described in Ochoa *et a*l. [24]. Briefly: 750,000 ECs were seeded per well of a 6 well plate (FN coated/BSA blocked as described earlier) and allowed to adhere for 75 minutes at 37°C before being moved to ice for 15 minutes. Cells were washed with PBS and then 100μl of PEM buffer (80 μM PIPES pH 6.8, 1 mM EGTA, 1 mM $MgCl_2$, 0.5% Triton X-100 and 25% (w/v) glycerol for 3 minutes. A second brief wash was performed with 50μl PEM buffer. All PEM buffer was collected and pooled together with 150μl EB buffer (3% SDS, 60 mM Sucrose, 65 mM Tris-HCL pH 6.8) at 2X concentration (representing cold soluble microtubules). Remaining material on the plate was then extracted using 300μl of EB buffer (representing cold stable microtubules). Samples were then used in western blotting analysis.

Additionally, the same procedure was used on ECs adhered to FN coated/BSA blocked coverslips (acid washed and bake-sterilised before coating). They were treated as above except after PEM washing the slides were immediately immersed in -20°C 100% methanol for 20 minutes. Coverslips were then used in immunolabelling analysis.

***In vivo* tumour growth assays**

The syngeneic mouse lung carcinoma cell line (derived from C57BL6 mice) CMT19T was used to grow subcutaneous tumours in β3 fl/fl Tie1Cre positive (and Cre negative littermate control) mice. Under anaesthetic, mice were injected subcutaneously in the flank with 1 x 10^6 cells. Tumours then grew for 7 days, at which point they were palpable through the skin, before the mice were treated with: (1) 0.15mg kg^{-1} Eribulin (kindly provided by Katherine Weilbaecher, Washington U) intravenously once a week for 2 weeks, or (2) 50mg kg^{-1} Fosbretabulin intraperitoneally every 4 days. After 21 days mice were culled and tumours were excised, photographed and measured for volume using a digital caliper. Tumours were bisected along the midline, fixed overnight in 4% paraformaldehyde, preserved for several days in cryoprotectant (20% sucrose, 2% poly(vinylpyrrolidone) in PBS), embedded in gelatin (8% gelatin, 20% sucrose, 2% poly(vinylpyrrolidone) in PBS) before being snap frozen and stored at -80°C.

Focal-adhesion and microtubule tracking

1 x 10^6 ECs were transfected with a GFP-tagged paxillin cDNA expression construct (provided by Maddy Parsons, KCL) by nucleofection. Cells were allowed to recover overnight before a fraction were seeded on FN coated/BSA blocked coverslips (acid washed and baked before coating) and adhered for 3 hours. Cells were then treated with 100nM SiRTubulin (Cytoskeleton Inc CY-SC002) and 1μM Verapamil overnight. Coverslips were imaged individually on an Axiovert (Zeiss) inverted microscope where one image of a GFP positive cell was taken every minute for 30 minutes at 37°C and 5% CO_2 in green and far-red channels. During imaging media was replaced with Phenol-red free OptiMEM® + 2% FBS containing 100nM SiRTubulin and 1μM Verapamil. The total area of adhesive fronts was assessed by measuring the growth of paxillin-GFP positive areas between the 1st and 30th image and then the number of microtubules that entered the adhesive front over 30 minutes were counted.

Western Blotting

For western blot analysis of total tubulin levels. ECs were seeded at 750,000 per well of a FN coated/BSA blocked 6 well plate and allowed to adhere for 90 minutes before being lysed in EB buffer. For the microtubule stability assay and focal adhesion enrichment samples were prepared as above. 20μg from each sample was loaded onto 10% polyacrylamide gels then transferred to a nitrocellulose membrane and incubated for 1 hour in 5% milk powder in PBS with 0.1% Tween 20 (PSBTw) followed by overnight incubation in primary antibody diluted 1:1000 in 5% BSA in PBSTw at 4°C. Primaries used were against integrin beta 3 (Cell Signalling 4702), alpha-tubulin (Abcam 7291), Gapdh (Abcam 9484), Rcc2 (Abcam 70788), Hspa1a (clone B-6 Santa Cruz Biotechnology), Anxa2 (Abcam 41803), and Itga5 (Cell Signalling 4705). The membranes were then incubated with the appropriate horseradish peroxidase (HRP)-conjugated secondary antibody (Dako) diluted 1:2000 in 5% milk in PBSTw for 1 hour at room temperature. The blot was visualised using Piece® ECL Western Blotting Substrate kit (ThermoFisher) and chemiluminescence detected on a Fujifilm LAS-3000 darkroom (Fujifilm UK Ltf, Beford, UK).

Immmunolabelleing cells

20,000 ECs were seeded onto FN coated/BSA blocked coverslips and adhered for 90 minutes before being washed with PBS and immersed in -20°C methanol for 20 minutes. Alternatively, cells were prepared as per the microtubule stability assay protocol above. Coverslips were then washed with PBS, blocked for 10 minutes at room temperature with 0.5% BSA, 1% goat serum in PBS with 0.25% Triton X-100 and incubated with primary antibody diluted 1:250 in PBS for 1 hour at room temperature. After subsequent PBS washes the coverslips were incubated with Alexa-Fluor® conjugated secondary antibodies raised in donkey (Fisher Scientific) diluted 1:500 in PBS. Coverslips were washed again in PBS before being mounted onto slides using Prolong Gold® with DAPI (Fisher Scientific). Primaries used were anti-alpha-tubulin (Abcam 52866), anti-paxillin (Abcam 32084) anti-talin (Sigma T3287), and anti-Nrp1 (R&D Systems AF566).

To quantify microtubule targeting focal adhesions, images were taken of stained cells using an epifluorescent microtubule then the number of microtubules with an end overlapping with a focal adhesion were counted for each cell.

Simultaneous Phalloidin (ThermoFisher A12380) and alpha-tubulin staining was carried out using PHEMO fixation [46].

Immunolabelling tissue sections

Five-μm cryosections were prepared from frozen tumours and stained as described previously [17]. Primaries used were anti-CD31 (R&D Systems AF3628, 1:500) and alpha-smooth muscle actin (Abcam 5694; 1:1000). Images were acquired on an Axioplan (Zeiss) epifluorescent microscope. Vessel density (immediately adjacent to, but not including, the tumour border) was measured by hand in 3 hot-spots per section. The area of each counted region was calculated using ImageJ.

siRNA knockdown

Knockdowns of Rcc2 and Anxa2 were achieved using 3μg of Dharmacon ON-TARGETplus SMARTpool siRNA (control smart pool used as knockdown control) per 1 x 10^6 ECs in an Amaxa Nucleofector II (T-005 setting). Cells were allowed to recover for 48 hours to allow knockdown to take effect.

Generation of human β3 integrin expressing cells

1X10^6 β3NULL endothelial cells were transfected with 10 μg of MfeI (New England Biolabs, Hitchin, UK) linearized full-length human β3-integrin (see Robinson *et al.*, 2009 [47]) cloned into pcDNA™6.2/C-EmGFP (see Amaxa nucleofections above). An empty vector (EV) was used as a control. Forty-eight hours post-transfection cells were selected with 10 μg ml^{-1} of blasticidin (ThermoFisher). Cells surviving 2 weeks were analysed for β3-integrin expression by western blotting.

Active Rac1 Pulldown

6 x 10^6 ECs were seeded onto FN coated/BSA blocked (as described above) 10 cm plates and allowed to adhere for 90 minutes. Rac1 Activation Magnetic Beads Pulldown Assay kit (Millipore 17-10393) was then used per manufacturer's instructions. Pull-down material was then loaded directly onto a gel for western blotting.

Rac1 Biosensor analyses

1 x 10^6 ECs were transfected with 10μg of Raichu-1011X (a gift from Maddy Parsons, KCL) via an Amaxa Nucleofector II (T-005 setting). Cells were allowed to recover for 48 hours, then plated onto FN coated/BSA blocked (as described above) coverslips for 90 minutes. Cells were fixed for 10 min in 4% PFA, then mounted in Prolong Gold® without DAPI (ThermoFisher).

Samples for analysis of the Rac FRET biosensor by acceptor photobleaching were imaged and analysed as previously described [48]. Briefly, images were acquired using an inverted Nikon A1R laser scanning confocal microscope. The CFP and YFP channels were excited using the 440nm diode laser and the 514nm argon line respectively. The two emission channels were split using a 545nm dichroic mirror, which was followed by a 475-525 nm bandpass filter for CFP and a 530nm longpass filter for YFP (Chroma). Pinholes were opened to give a depth of focus of 2 μm for each channel. Scanning was performed on a sequential line-by-line basis for each channel. The gain for each channel was set to approximately 75 % of dynamic range (12-bit, 4096 grey levels) and offsets set such that backgrounds were zero. Time-lapse mode was used to collect one pre-bleach image for each channel followed by bleaching with a minimum of 20 iterations of the 514nm argon laser line at maximum power (to bleach YFP). A second post-bleach image was then collected for each channel. Control non-bleached areas were acquired for all samples in the same field of view as bleached cells to confirm specificity of FRET detection. Pre- and post-bleach TFP and Venus images were then imported into Image J for processing. Briefly, images were smoothed using a 3 x 3 box mean filter, background subtracted and post-bleach images fade compensated. A FRET efficiency ratio map over the whole cell was calculated using the following formula: $(TFP_{postbleach}-TFP_{prebleach})/TFP_{postbleach}$. Ratio values were then extracted from pixels falling inside the bleach region as well as an equally sized region outside of the bleach region and the mean ratio determined for each region and plotted on a histogram. The non-bleach ratio was then subtracted from the bleach region ratio to give a final value for the FRET efficiency ratio. Data from images were used only if YFP bleaching efficiency was greater than 70%.

Statistical Analyses

All statistical tests were performed using GraphPad Prism^{TM} Software. Significant differences between means were evaluated by unpaired two-tailed student's *t* test. $P<0.05$ was considered statistically significant. Exact *P* values are shown on figures, except where $P<0.0001$; ns= $P>0.05$.

Data availability

The mass spectrometry proteomics data have been deposited to the ProteomeXchange Consortium via the PRIDE [49] partner repository with the dataset identifier PXD008591.

Acknowledgements

Special thanks to both Drs Sophie Akbareian and Peng Liu for their undying enthusiastic and critical support of this project. Additionally, we thank Norfolk Fundraisers and Mrs Margaret Doggett for their kind support and fundraising over the years.

Author Contributions

Atkinson designed and performed experiments, analyzed data, and helped write and edit the manuscript. Gontarczyk, Ellison, Johnson, Harry, and Parsons designed and performed experiments, analyzed data, and helped edit the manuscript. Kirkup, Alghamdi, Fowler, Silva performed experiments, analyzed data, and helped edit the manuscript. Schneider, Weilbaecher and Bass provided essential data and helped edit the manuscript. Mogensen and Edwards analyzed data and helped edit the manuscript. Robinson designed experiments, performed experiments, analyzed data, and wrote the manuscript.

Conflict of Interest

The authors declare no competing financial interests.

References

1. Hanahan D, Weinberg RA (2011) Hallmarks of cancer: the next generation. *Cell* **144**: 646-74

2. Zhao Y, Adjei AA (2015) Targeting Angiogenesis in Cancer Therapy: Moving Beyond Vascular Endothelial Growth Factor. *Oncologist* **20**: 660-73

3. Chen CT, Hung MC (2013) Beyond anti-VEGF: dual-targeting antiangiogenic and antiproliferative therapy. *American journal of translational research* **5**: 393-403

4. Brooks PC, Clark RA, Cheresh DA (1994) Requirement of vascular integrin alpha v beta 3 for angiogenesis. *Science* **264**: 569-71

5. Kim S, Bell K, Mousa SA, Varner JA (2000) Regulation of angiogenesis in vivo by ligation of integrin alpha5beta1 with the central cell-binding domain of fibronectin. *Am J Pathol* **156**: 1345-62

6. Reynolds LE, Wyder L, Lively JC, Taverna D, Robinson SD, Huang X, Sheppard D, Hynes RO, Hodivala-Dilke KM (2002) Enhanced pathological angiogenesis in mice lacking beta3 integrin or beta3 and beta5 integrins. *Nat Med* **8**: 27-34

7. Steri V, Ellison TS, Gontarczyk AM, Weilbaecher K, Schneider JG, Edwards D, Fruttiger M, Hodivala-Dilke KM, Robinson SD (2014) Acute depletion of endothelial beta3-integrin transiently inhibits tumor growth and angiogenesis in mice. *Circ Res* **114**: 79-91

8. Murphy PA, Begum S, Hynes RO (2015) Tumor angiogenesis in the absence of fibronectin or its cognate integrin receptors. *PLoS One* **10**: e0120872

9. Schaffner F, Ray AM, Dontenwill M (2013) Integrin alpha5beta1, the Fibronectin Receptor, as a Pertinent Therapeutic Target in Solid Tumors. *Cancers (Basel)* **5**: 27-47

10. Stupp R, Hegi ME, Gorlia T, Erridge SC, Perry J, Hong YK, Aldape KD, Lhermitte B, Pietsch T, Grujicic D*, et al.* (2014) Cilengitide combined with standard treatment for patients with newly diagnosed glioblastoma with methylated MGMT promoter (CENTRIC EORTC 26071-22072 study): a multicentre, randomised, open-label, phase 3 trial. *Lancet Oncol* **15**: 1100-8

11. Hynes RO (2002) Integrins: bidirectional, allosteric signaling machines. *Cell* **110**: 673-87

12. Horton ER, Byron A, Askari JA, Ng DH, Millon-Fremillon A, Robertson J, Koper EJ, Paul NR, Warwood S, Knight D*, et al.* (2015) Definition of a consensus integrin adhesome and its dynamics during adhesion complex assembly and disassembly. *Nat Cell Biol* **17**: 1577-87

13. Schiller HB, Friedel CC, Boulegue C, Fassler R (2011) Quantitative proteomics of the integrin adhesome show a myosin II-dependent recruitment of LIM domain proteins. *EMBO Rep* **12**: 259-66

14. Zaidel-Bar R, Itzkovitz S, Ma'ayan A, Iyengar R, Geiger B (2007) Functional atlas of the integrin adhesome. *Nat Cell Biol* **9**: 858-67

15. May T, Mueller PP, Weich H, Froese N, Deutsch U, Wirth D, Kroger A, Hauser H (2005) Establishment of murine cell lines by constitutive and conditional immortalization. *Journal of biotechnology* **120**: 99-110

16. Schiller HB, Hermann MR, Polleux J, Vignaud T, Zanivan S, Friedel CC, Sun Z, Raducanu A, Gottschalk KE, Thery M*, et al.* (2013) beta1- and alphav-class integrins cooperate to regulate myosin II during rigidity sensing of fibronectin-based microenvironments. *Nat Cell Biol* **15**: 625-36

17. Ellison TS, Atkinson SJ, Steri V, Kirkup BM, Preedy ME, Johnson RT, Ruhrberg C, Edwards DR, Schneider JG, Weilbaecher K*, et al.* (2015) Suppressing beta3-integrin triggers a neuropilin-1 dependent change in focal adhesion remodelling that can be targeted to block pathological angiogenesis. *Dis Model Mech* **8**: 1105-1119

18. Kaverina I, Straube A (2011) Regulation of cell migration by dynamic microtubules. *Seminars in cell & developmental biology* **22**: 968-74

19. Jordan MA, Kamath K, Manna T, Okouneva T, Miller HP, Davis C, Littlefield BA, Wilson L (2005) The primary antimitotic mechanism of action of the synthetic halichondrin E7389 is suppression of microtubule growth. *Molecular cancer therapeutics* **4**: 1086-95

20. Dorr RT, Dvorakova K, Snead K, Alberts DS, Salmon SE, Pettit GR (1996) Antitumor activity of combretastatin-A4 phosphate, a natural product tubulin inhibitor. *Invest New Drugs* **14**: 131-7

21. Su X, Esser AK, Amend SR, Xiang J, Xu Y, Ross MH, Fox GC, Kobayashi T, Steri V, Roomp K*, et al.* (2016) Antagonizing Integrin beta3 Increases Immunosuppression in Cancer. *Cancer Res* **76**: 3484-95

22. Morgan EA, Schneider JG, Baroni TE, Uluckan O, Heller E, Hurchla MA, Deng H, Floyd D, Berdy A, Prior JL*, et al.* (2010) Dissection of platelet and myeloid cell defects by conditional targeting of the beta3-integrin subunit. *Faseb J* **24**: 1117-27

23. Gustafsson E, Brakebusch C, Hietanen K, Fassler R (2001) Tie-1-directed expression of Cre recombinase in endothelial cells of embryoid bodies and transgenic mice. *Journal of cell science* **114**: 671-6

24. Ochoa CD, Stevens T, Balczon R (2011) Cold exposure reveals two populations of microtubules in pulmonary endothelia. *Am J Physiol Lung Cell Mol Physiol* **300**: L132-8

25. Humphries JD, Byron A, Bass MD, Craig SE, Pinney JW, Knight D, Humphries MJ (2009) Proteomic analysis of integrin-associated complexes identifies RCC2 as a dual regulator of Rac1 and Arf6. *Sci Signal* **2**: ra51

26. Mollinari C, Reynaud C, Martineau-Thuillier S, Monier S, Kieffer S, Garin J, Andreassen PR, Boulet A, Goud B, Kleman JP*, et al.* (2003) The mammalian passenger protein TD-60 is an RCC1 family member with an essential role in prometaphase to metaphase progression. *Dev Cell* **5**: 295-307

27. Williamson RC, Cowell CA, Hammond CL, Bergen DJ, Roper JA, Feng Y, Rendall TC, Race PR, Bass MD (2014) Coronin-1C and RCC2 guide mesenchymal migration by trafficking Rac1 and controlling GEF exposure. *J Cell Sci* **127**: 4292-307

28. Hansen MD, Ehrlich JS, Nelson WJ (2002) Molecular mechanism for orienting membrane and actin dynamics to nascent cell-cell contacts in epithelial cells. *J Biol Chem* **277**: 45371-6

29. Daub H, Gevaert K, Vandekerckhove J, Sobel A, Hall A (2001) Rac/Cdc42 and p65PAK regulate the microtubule-destabilizing protein stathmin through phosphorylation at serine 16. *J Biol Chem* **276**: 1677-80

30. Banerjee M, Worth D, Prowse DM, Nikolic M (2002) Pak1 phosphorylation on t212 affects microtubules in cells undergoing mitosis. *Curr Biol* **12**: 1233-9

31. Wittmann T, Bokoch GM, Waterman-Storer CM (2004) Regulation of microtubule destabilizing activity of Op18/stathmin downstream of Rac1. *J Biol Chem* **279**: 6196-203

32. Palamidessi A, Frittoli E, Garre M, Faretta M, Mione M, Testa I, Diaspro A, Lanzetti L, Scita G, Di Fiore PP (2008) Endocytic trafficking of Rac is required for the spatial restriction of signaling in cell migration. *Cell* **134**: 135-47

33. D'Amico G, Robinson SD, Germain M, Reynolds LE, Thomas GJ, Elia G, Saunders G, Fruttiger M, Tybulewicz V, Mavria G*, et al.* (2010) Endothelial-Rac1 is not required for tumor angiogenesis unless alphavbeta3-integrin is absent. *PLoS One* **5**: e9766

34. Worth DC, Hodivala-Dilke K, Robinson SD, King SJ, Morton PE, Gertler FB, Humphries MJ, Parsons M (2010) Alpha v beta3 integrin spatially regulates VASP and RIAM to control adhesion dynamics and migration. *J Cell Biol* **189**: 369-83

35. Byron A, Askari JA, Humphries JD, Jacquemet G, Koper EJ, Warwood S, Choi CK, Stroud MJ, Chen CS, Knight D*, et al.* (2015) A proteomic approach reveals integrin activation state-dependent control of microtubule cortical targeting. *Nat Commun* **6**: 6135

36. Fukata M, Watanabe T, Noritake J, Nakagawa M, Yamaga M, Kuroda S, Matsuura Y, Iwamatsu A, Perez F, Kaibuchi K (2002) Rac1 and Cdc42 capture microtubules through IQGAP1 and CLIP-170. *Cell* **109**: 873-85

37. Reynolds AR, Reynolds LE, Nagel TE, Lively JC, Robinson SD, Hicklin DJ, Bodary SC, Hodivala-Dilke KM (2004) Elevated Flk1 (vascular endothelial growth factor receptor 2) signaling mediates enhanced angiogenesis in beta3-integrin-deficient mice. *Cancer Res* **64**: 8643-50

38. Mahabeleshwar GH, Feng W, Reddy K, Plow EF, Byzova TV (2007) Mechanisms of integrin-vascular endothelial growth factor receptor cross-activation in angiogenesis. *Circ Res* **101**: 570-80

39. Turaga RC, Yin L, Yang JJ, Lee H, Ivanov I, Yan C, Yang H, Grossniklaus HE, Wang S, Ma C*, et al.* (2016) Rational design of a protein that binds integrin alphavbeta3 outside the ligand binding site. *Nat Commun* **7**: 11675

40. Krilleke D, Deerkenez A, Schubert W, Giri I, Robinson GS, Ng YS, Shima DT (2007) Molecular mapping and functional characterization of the VEGF164 heparin-binding domain. *J Biol Chem* **282**: 280450-280456

41. Reynolds LE, Hodivala-Dilke KM (2006) Primary mouse endothelial cell culture for assays of angiogenesis. *Methods Mol Med* **120**: 503-9

42. Cox J, Mann M (2008) MaxQuant enables high peptide identification rates, individualized p.p.b.-range mass accuracies and proteome-wide protein quantification. *Nat Biotechnol* **26**: 1367-72

43. Tyanova S, Temu T, Sinitcyn P, Carlson A, Hein MY, Geiger T, Mann M, Cox J (2016) The Perseus computational platform for comprehensive analysis of (prote)omics data. *Nat Methods* **13**: 731-40

44. Tusher VG, Tibshirani R, Chu G (2001) Significance analysis of microarrays applied to the ionizing radiation response. *Proc Natl Acad Sci U S A* **98**: 5116-21

45. Meijering E, Dzyubachyk O, Smal I (2012) Methods for cell and particle tracking. *Methods Enzymol* **504**: 183-200

46. Bellett G, Carter JM, Keynton J, Goldspink D, James C, Moss DK, Mogensen MM (2009) Microtubule plus-end and minus-end capture at adherens junctions is involved in the assembly of apico-basal arrays in polarised epithelial cells. *Cell Motil Cytoskeleton* **66**: 893-908

47. Robinson SD, Reynolds LE, Kostourou V, Reynolds AR, da Silva RG, Tavora B, Baker M, Marshall JF, Hodivala-Dilke KM (2009) Alphav beta3 integrin limits the contribution of neuropilin-1 to vascular endothelial growth factor-induced angiogenesis. *J Biol Chem* **284**: 33966-81

48. Scarpa E, Szabo A, Bibonne A, Theveneau E, Parsons M, Mayor R (2015) Cadherin Switch during EMT in Neural Crest Cells Leads to Contact Inhibition of Locomotion via Repolarization of Forces. *Dev Cell* **34**: 421-34

49. Vizcaino JA, Csordas A, del-Toro N, Dianes JA, Griss J, Lavidas I, Mayer G, Perez-Riverol Y, Reisinger F, Ternent T*, et al.* (2016) 2016 update of the PRIDE database and its related tools. *Nucleic Acids Res* **44**: D447-56

Figure Legends

Figure 1. Defining the FN endothelial adhesome.

A) WT ECs were adhered to fibronectin (top row) or poly-l-lysine (bottom row) coated coverslips for 90 minutes before fixing and immunostaining for neuropilin-1 (Nrp1-green) and talin-1 (Tln1-red) along with a nuclear stain (DAPI-blue). Scale bar = 10µm.

B) An example silver stain used in the quality control of adhesome samples. Adhesome enrichment was carried out on 6 x 10^6 WT ECs on fibronectin (FN), fibronectin with VEGF (FN + VEGF) or poly-l-lysine (PLL) before acetone precipitation. After resuspension samples were run on a SDS-PAGE gel along with a whole cell lysate control and silver stained.

C) Triplicate adhesome samples from WT ECs adhered on fibronectin (FN), fibronectin with VEGF (FN + VEGF) or poly-l-lysine were sent for quantitative mass spec analysis. Label free quantification was carried out using MaxQuant followed by analysis in Perseus. Unsupervised hierarchical clustering (Euclidian distance calculation) was carried out with red showing highly abundant proteins and green showing low abundance proteins. 12 significant clusters were automatically identified using a distance threshold of 3.34 and labelled A-L. Angiogenesis associated proteins were identified using GOBP annotations (GO:0001525, GO:0002040, GO:0002042, GO:0016525, GO:0045765, GO:0045766) and are displayed in the table along with their associated cluster.

Figure 2. Analysis of the β3-integrin dependent adhesome.

A) Distribution of adhesion size classes (0-2µm, 2-10µm; >10µm) in β3WT versus β3HET endothelial cells (n=1400 FAs per genotype; 2 independent experiments).

B) Visual representation of the significant analysis of microarrays (SAM) method as a volcano plot for β3WT and β3HET samples (n=3). T-test difference is plotted against –log of the P value. The blue lines show the cut-off for significance as defined by the SAM. Integrin-β3 (Itgb3) as well as all detected tubulins (Tub) have been highlighted as red points.

C) Adhesome samples from β3WT and β3HET endothelial cells adhered to fibronectin. Samples were western blotted for integrin-β3 (Itgb3), α-tubulin and heat shock protein 70 (Hspa1a). Blot shown is representative of the 5 individual experiments that are quantified in the bar graph below. Bars = mean (±SEM) relative α-tubulin levels normalised to Hspa1a levels.

Figure 3. Analysis of microtubules in β3WT, β3HET and β3NULL endothelial cells.

A) β3WT, β3HET and β3NULL endothelial cells were adhered to fibronectin coated coverslips for 90 minutes before being PHEMO fixed and immunostained for α-tubulin (green). Nuclear (DAPI-blue) and Phallodin (F-actin - red) stains were also used. Inverted black and white images of α-tubulin and F-actin are shown below the three-colour overlays. Scale bar = 10μm.

B) β3WT, β3HET and β3NULL endothelial cells were adhered to fibronectin for 90 minutes before being lysed and western blotted for Integrin-β3 (Itgb3), α-tubulin and Gapdh (as a loading control).

C) *Left* β3WT, β3HET and β3NULL endothelial cells were adhered to fibronectin coated coverslips for 90 minutes before being methanol (-20°C) fixed and immunostained for α-tubulin and talin-1. The number of microtubules that terminated (overlapping staining) at a talin-1 containing focal adhesion were counted for each genotype (n=15 cells per genotype, from 3 independent experiments). *Right* β3 WT, HET and NULL ECS were transfected with paxillin-GFP and left to recover overnight. The cells were then adhered to fibronectin coated coverslips and allowed to recover for 3 hours before being treated with 100 nM SiRTubulin and 1 μM verapamil overnight. The next day, fresh media containing SiRTubulin and verampamil (same dose) was added and cells were imaged every minute for 30 minutes (n=3 cells per genotype, from 3 independent experiments). Areas of adhesive fronts were assessed by measuring the growth of paxillin-GFP positive areas between the 1st and 30th image. The number of microtubules that entered the adhesive front was quantified to give the number of microtubules entering lamellipodia relative to the area of adhesive fronts for each cell.

D) β3WT, β3HET and β3NULL endothelial cells were adhered to fibronectin overnight. Migration speed of individual cells was measured over 15 hours using the MTrackJ plugin for ImageJ whilst under the influence of the indicated MTA. Migration speeds are shown as a percentage of the speed of the corresponding genotype under DMSO (vehicle) treatment (n≥46 cells per genotype, from 4 independent experiments).

E) β3flox/flox Tie1Cre positive (pos) and negative (neg) animals were injected subcutaneously with 1X10^6 CMT19T lung carcinoma cells and then treated with vehicle (veh), or Eribulin (Eri). Bar graph shows mean (±SEM) tumour volumes (n≥6; from 2-3 independent experiments for each treatment condition) at the end of the experiment. Micrographs (below) show representative tumours. Scale bars = 5mm.

F) After excision, tumours from β3flox/flox Tie1Cre positive (pos) and negative (neg) animals were processed and CD31 staining was assessed in vessel hotspots (see materials and methods) to measure vascular density. Bars = mean (±SEM) vessel number per mm^2 (n=5 sections from each genotype, taken over 2-3 independent experiments for each treatment condition). Micrographs (below) show representative images of sections stained for alpha smooth muscle actin (αSMA=green), CD31 (red), DAPI (blue). Dotted white line indicates border of tumour and surrounding connective tissue. Scale bars = 100μm.

Figure 4. Analysis of microtubule stability in β3WT, β3HET and β3NULL endothelial cells.

A) *Top* β3WT, β3HET and β3NULL endothelial cells were adhered to fibronectin coated coverslips for 75 minutes at 37°C before being moved to ice for 15 minutes. Soluble tubulin was then washed out using PEM buffer (see materials and methods) before fixing with -20°C methanol (Note: this protocol leads to nuclear auto-fluorescent background in all three channels used). Immunostaining was carried out for α-tubulin (green) and Talin-1 (Tln1-red). DAPI (blue) was used as a nuclear stain. Images shown are representative of the data shown in the bar graph shown below. Scale bar = 5 μm. *Bottom* dot plots = mean (±SEM) number of cold-stable microtubules per cell (n ≥ 300 cells per genotype, from 3 independent experiments).

B) β3WT, β3HET and β3NULL endothelial cells were adhered to fibronectin for 75 minutes at 37°C before being moved to ice for 15 minutes. Cold-soluble tubulin (*Left blot*) was then washed out using PEM buffer and western blotted for α-tubulin and Gapdh (as a loading control). Cold-insoluble tubulin (*Middle blot*) from the same cells was obtained by then lysing the remaining cells and western blotting for α-tubulin and Gapdh (as a loading control). *Right bar chart* Bars = mean (±SEM) relative cold-soluble and cold-insoluble α-tubulin levels for each genotype. Data are representative of 4 independent experiments. * indicates statistical significance compared to WT (P<0.05).

Figure 5. Microtuble stability in endothelial cells is regulated by Itgb3, Rcc2, Anxa2, and Rac1.

A) β3WT ECs were transfected with control pool (CP) or Rcc2 smart pool siRNA and allowed to recover for 48 hours. They were then adhered to fibronectin coated coverslips for 75 minutes at 37°C before being moved to ice for 15 minutes. Soluble tubulin was then washed out using PEM buffer before fixing with -20°C methanol. Immunostaining was carried out for α-tubulin to allow counting of the number of cold stable microtubules per cell. *Left* Western blot showing representative Rcc2 knockdown. Gapdh is shown as a loading control. *Right* Bars = mean (±SEM) number of cold stable microtubules shown as a percentage relative to CP treated cells ($n \geq 455$ cells per condition, from 3 independent experiments).

B) β3WT ECs were transfected with control pool (CP) or Anxa2 smart pool siRNA and allowed to recover for 48 hours. They were then adhered to fibronectin coated coverslips for 75 minutes at 37°C before being moved to ice for 15 minutes. Soluble tubulin was then washed out using PEM buffer before fixing with -20°C methanol. Immunostaining was carried out for α-tubulin to allow counting of the number of cold stable microtubules per cell. *Top* Western blot showing representative Anxa2 knockdown in 3 separate samples. *Bottom Left* Bars = mean (±SEM) Anxa2 knockdown shown as a percentage relative to CP treated cells. Samples have been normalised to Hspa1a. *Bottom Right* Bars = mean (±SEM) number of cold stable microtubules shown as a percentage relative to CP treated cells ($n \geq 450$ cells per condition, from 3 independent experiments).

C) β3WT, β3HET and β3NULL endothelial cells were adhered to fibronectin coated coverslips for 60 minutes at 37°C before being treated with DMSO (control) or 50 μM NSC23766 and incubated at 37°C for a further 15 minutes. Coverslips were moved to ice for 15 minutes. Soluble tubulin was then washed out using PEM buffer before fixing with -20°C methanol. Immunostaining was carried out for alpha-tubulin to allow counting of the number of cold stable microtubules per cell. Bars = mean (±SEM) number of microtubules per cell shown as a percentage relative to DMSO treated controls (n=218 cells per condition, from 2 independent experiments).

D) β3WT, β3HET and β3NULL endothelial cells were adhered to fibronectin for 90 minutes before being lysed and western blotted for Integrin-β3 (Itgb3), Rac1 and Hspa1a (as a loading control). Blot shown is representative of 3 individual experiments.

E) β3WT, β3HET and β3NULL endothelial cells were adhered to fibronectin coated plates for 90 minutes before being lysed in MLB (see materials and methods). GTP-

Rac1 and bound proteins were extracted from cleared MLB using PAK-1 PBD magnetic beads at 4°C for an hour before being western blotted for Itga5, Itgb3, Rcc2, Anxa2 and Rac1. Blot is representative of at least 3 independent experiments *Right* Bars = mean (±SD) level of association of the indicated protein with GTP-Rac1, shown relative to β3WT associations (and normalized to the level of active Rac1 pulled down). Results are from at least 3 independent experiments.

F) β3WT, β3HET and β3NULL endothelial cells were transfected with a Raichu-Rac1 biosensor. After 48 hours, cells were adhered to fibronectin coated plates for 90 minutes, then fixed in PFA. *Left* FRET-efficiency was measured as described in materials and methods. Graph shows mean FRET efficiencies (±SEM) (n=17 cells per genotype; 2 independent experiments). *Right* Representative images showing spatial distribution of Rac1 FRET efficiency in β3WT, β3HET and β3NULL endothelial cells (white stars indicate cytoplasmic localisation of active Rac1 in β3HET and β3NULL). Scale bar = 5μm.

Expanded View Figure Legends

Figure EV1. A Schematic demonstrating how figure 3C (right) was calculated. The yellow line indicates the edge of Pxn-GFP (green) positive areas at 0 minutes and the blue line indicates the edge at the end of 30 minutes. Microtubules were labelled red with SiR Tubulin. Scale bar = 5 μm.

Figure EV2. β3WT, β3HET and β3NULL endothelial cells were adhered to fibronectin overnight. Migration speed of individual cells was measured over 15 hours using the MTrackJ plugin for ImageJ whilst under the influence of the indicated MTA. Bars = mean migration speed (±SEM) (n≥46 cells per genotype, from 4 independent experiments).

Figure EV3 *Top* β3NULL endothelial cells were transfected with a full-length human β3-integrin (hβ3) cDNA expression construct or an empty vector (EV) control and western blotted for β3-integrin (β3NULL parent cells shown for comparison). *Bottom* β3NULL+EV or β3NULL+hβ3 endothelial cells were adhered to fibronectin coated coverslips for 75 minutes at 37°C before being moved to ice for 15 minutes. Soluble tubulin was then washed out using PEM buffer (see materials and methods) before fixing with -20°C methanol. Immunostaining was carried out for α-tubulin (green) and Talin-1 (Tln1-red). DAPI (blue) was used as a nuclear stain. Images shown are representative of the data shown in the bar graph above. Bars = mean (±SEM) number of cold-stable microtubules per cell. Scale bar = 5 μm. (n=96 cells per genotype).

Figure EV4. *Top* β3WT ECs were transfected with control pool (CP), Anxa2 smart pool siRNA, Rcc2 smart pool siRNA, or both and allowed to recover for 48 hours. They were then adhered to fibronectin coated coverslips for 75 minutes at 37°C before being moved to ice for 15 minutes. Soluble tubulin was then washed out using PEM buffer before fixing with -20°C methanol. Immunostaining was carried out for α-tubulin (green) and Talin-1 (Tln1-red). DAPI (blue) was used as a nuclear stain. Scale bar = 5μm. *Bottom* β3WT, β3HET and β3NULL cells were adhered to fibronectin coated coverslips for 60 minutes at 37°C before treated with DMSO or 50 μM NSC23766 and incubated at 37°C for a further 15 minutes. Cells were then moved to ice for 15 minutes. Soluble tubulin was washed out using PEM buffer before fixing with -20°C methanol. Immunostaining was carried out for α-tubulin (green) and Talin-1 (Tln1-red). DAPI (blue) was used as a nuclear stain. Scale bar = 5 μm.

Figure EV5. *Top* β3WT endothelial cells were transfected with control pool (CP), Anxa2, or Rcc2 smart pool siRNA and allowed to recover for 48 hours. Cells were then adhered to fibronectin coated coverslips for 60 minutes at 37°C before treated with DMSO (veh) or 50 μM NSC23766 (+) and incubated at 37°C for a further 15 minutes. Coverslips were moved to ice for 15 minutes. Soluble tubulin was then washed out using PEM buffer before fixing with -20°C methanol. Immunostaining was carried out for alpha-tubulin to allow counting of the number of cold stable microtubules per cell. Bars = mean (±SEM) number of microtubules per cell shown as a percentage relative to the CP/veh control (n=100 cells per condition, from 2 independent experiments). Scale bar = 5 μm.

Figure 1

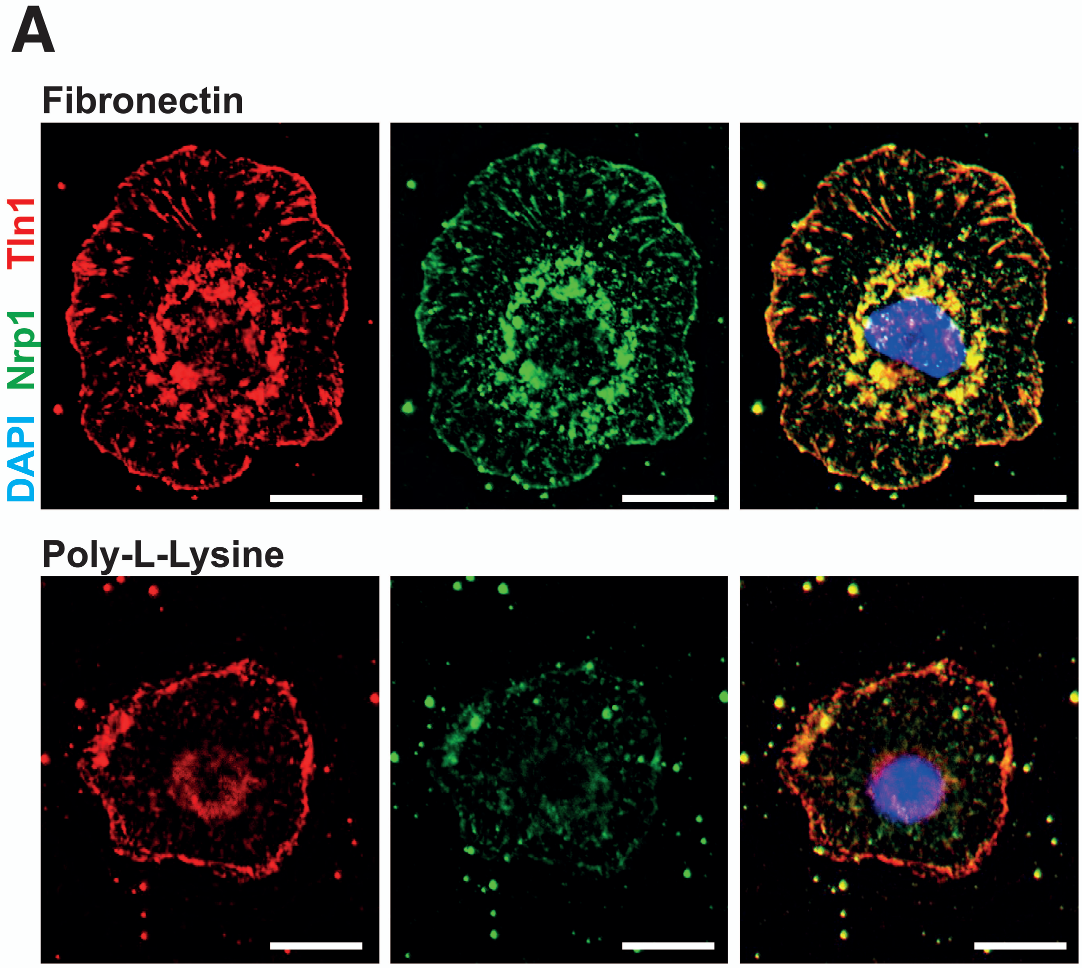

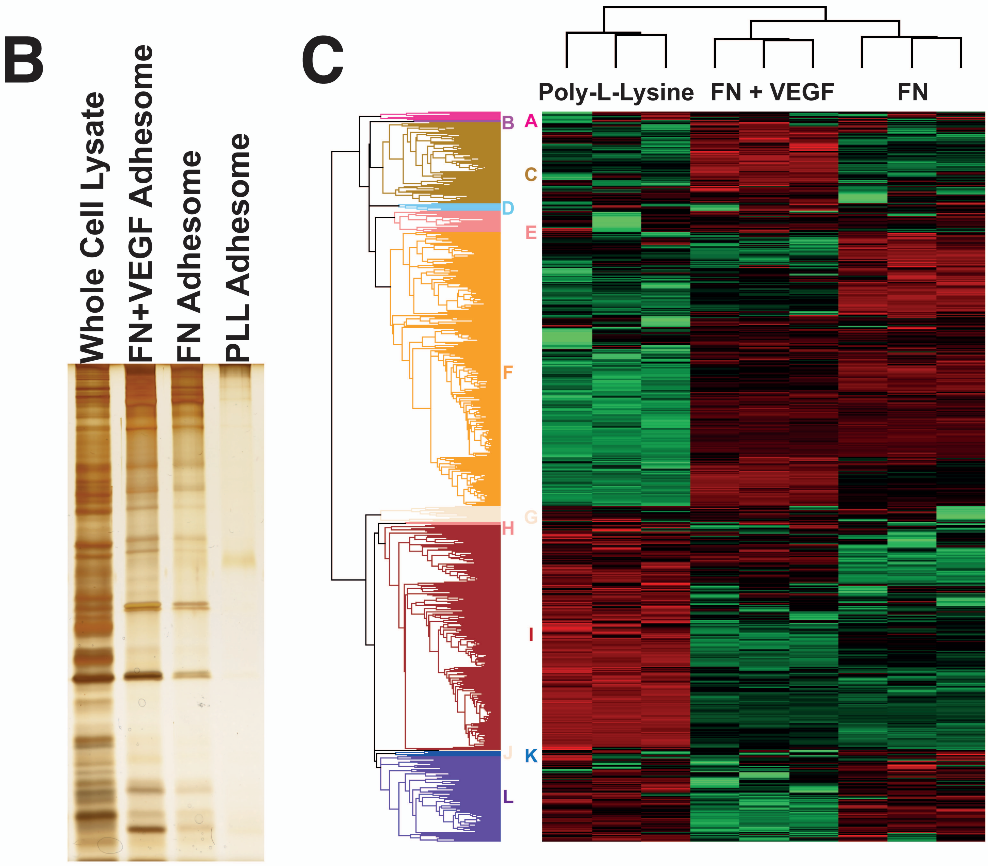

Cluster	Gene names	Cluster	Gene names
A	Parva	F	Itgav
C	Eng	F	Tie1
C	Atp5b	F	Ecm1
C	Cyr61	F	Ephb4
C	Epha2	F	Thbs1
C	Myh9	F	Ptprb
C	Rtn4	F	Itgb3
C	Nrp2	F	Mmrn2
C	Cdc42	F	Anxa2
D	Map1b	F	Mcam
E	Cav1	F	Mfge8
E	Rock2	F	Itgb1
E	Stat1	F	Stab1
F	Mtdh	F	Wasf2
F	Srpk2	F	Sp100
F	Ptk2	F	Nos3
F	Rnh1	G	Col18a1
F	Gtf2i	I	Naa15
F	Col4a2	I	Ctgf
F	Rasip1	I	Pdcd6
F	Serpine1	I	Hspg2
F	Loxl2	I	Anxa3
F	Nrp1	L	Vash1
F	Ncl	L	Flt1

Figure 2

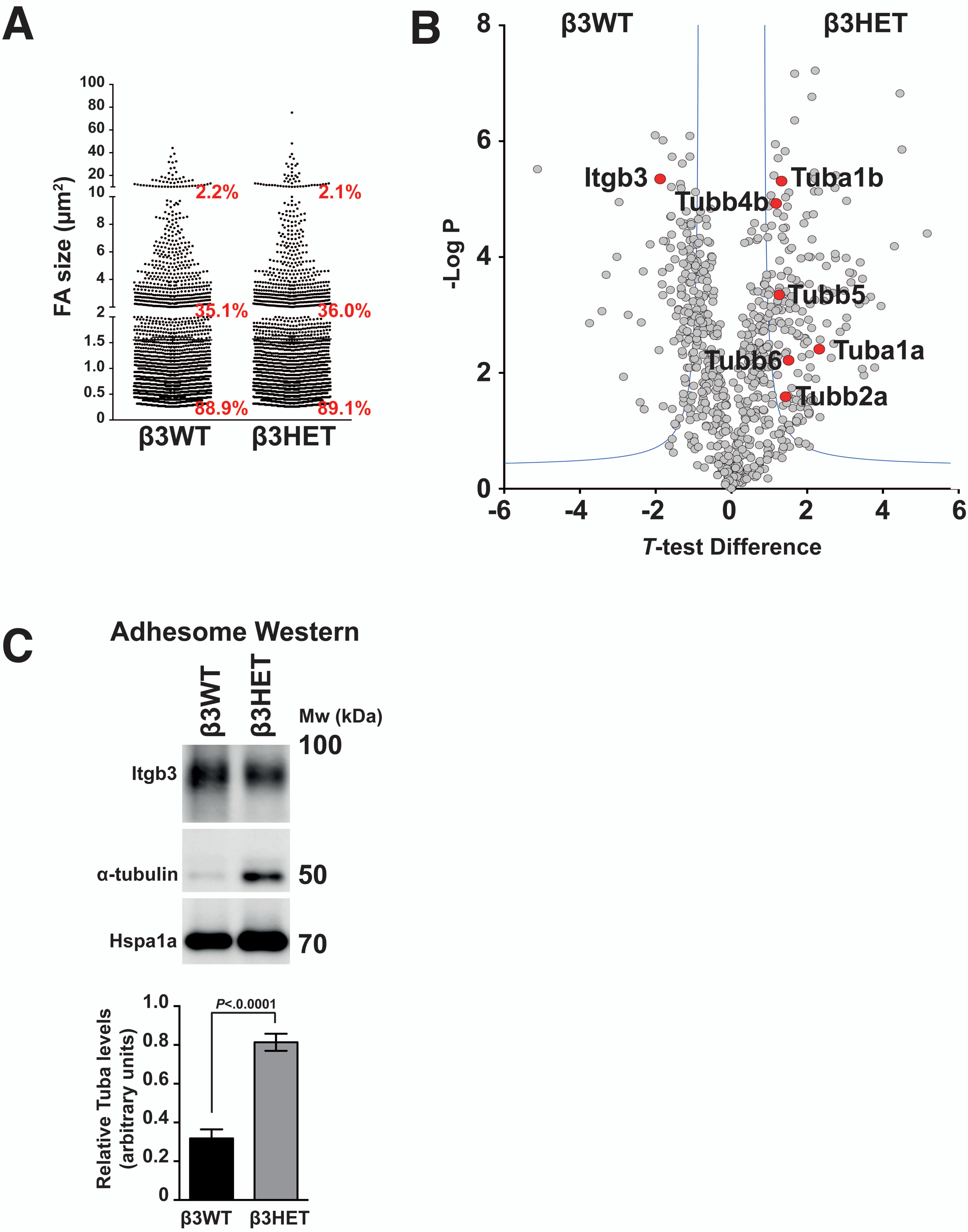

A
FA size (μm²)
100
80
60
40
20
10
8
6
4
2
1.5
1.0
0.5
0
2.2%
2.1%
35.1%
36.0%
88.9%
89.1%
β3WT
β3HET
B
β3WT
β3HET
-Log P
T-test Difference
Itgb3
Tuba1b
Tubb4b
Tubb5
Tuba1a
Tubb6
Tubb2a
C
Adhesome Western
β3WT
β3HET
Mw (kDa)
Itgb3
100
α-tubulin
50
Hspa1a
70
Relative Tuba levels (arbitrary units)
P<.0.0001
1.0
0.8
0.6
0.4
0.2
0
β3WT
β3HET

Figure 3

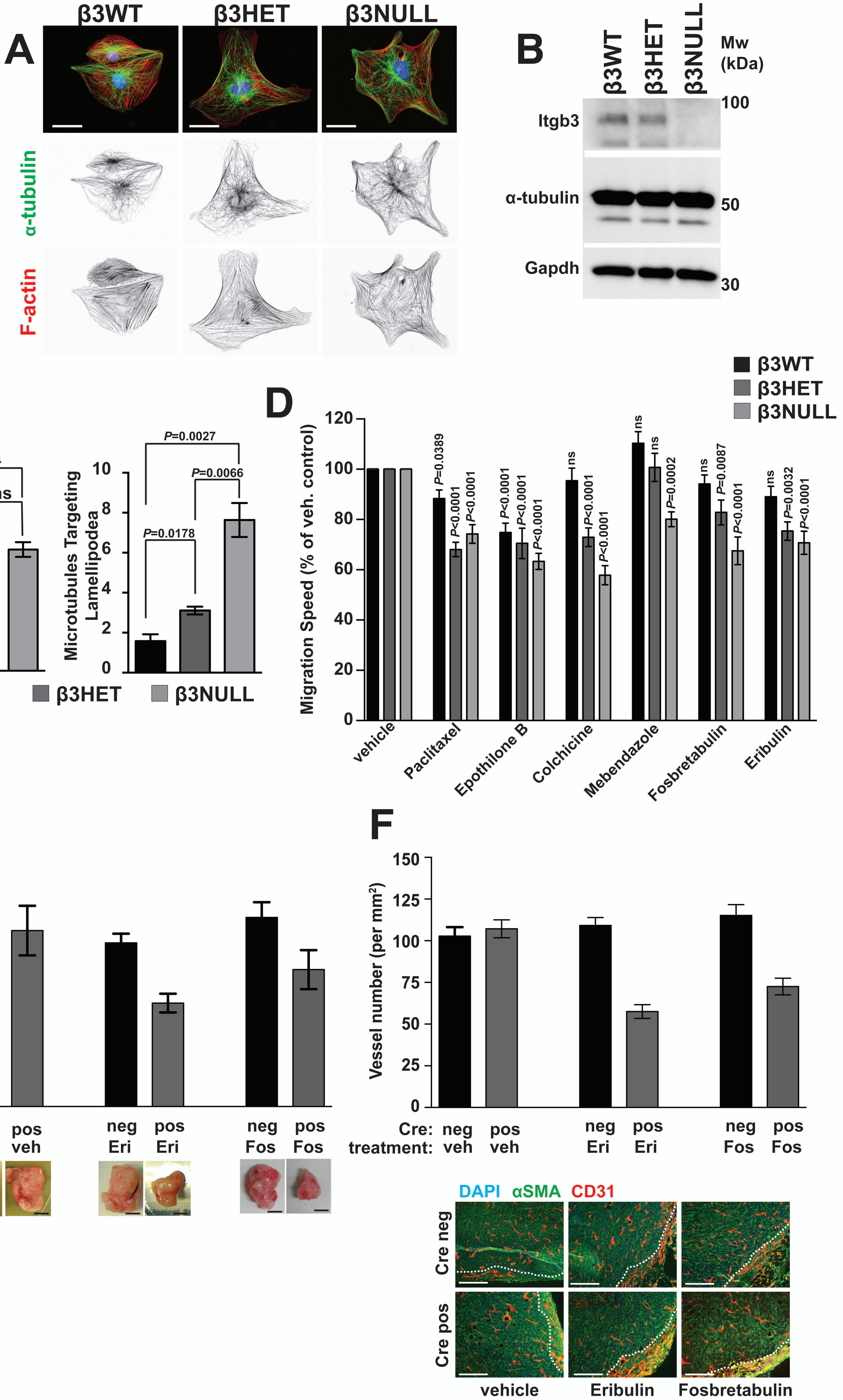

A
β3WT
β3HET
β3NULL
α-tubulin
F-actin
B
Mw (kDa)
Itgb3
α-tubulin
Gapdh
100
50
30
C
Microtubules Targeting Peripheral Focal Adhesions
P=0.004
P=0.0006
ns
Microtubules Targeting Lamellipodea
P=0.0027
P=0.0066
P=0.0178
D
Migration Speed (% of veh. control)
vehicle
Paclitaxel
Epothilone B
Colchicine
Mebendazole
Fosbretabulin
Eribulin
E
Tumour volume (mm³)
Cre:
treatment:
neg veh
pos veh
neg Eri
pos Eri
neg Fos
pos Fos
F
Vessel number (per mm²)
DAPI αSMA CD31
Cre neg
Cre pos
vehicle
Eribulin
Fosbretabulin

Figure 4

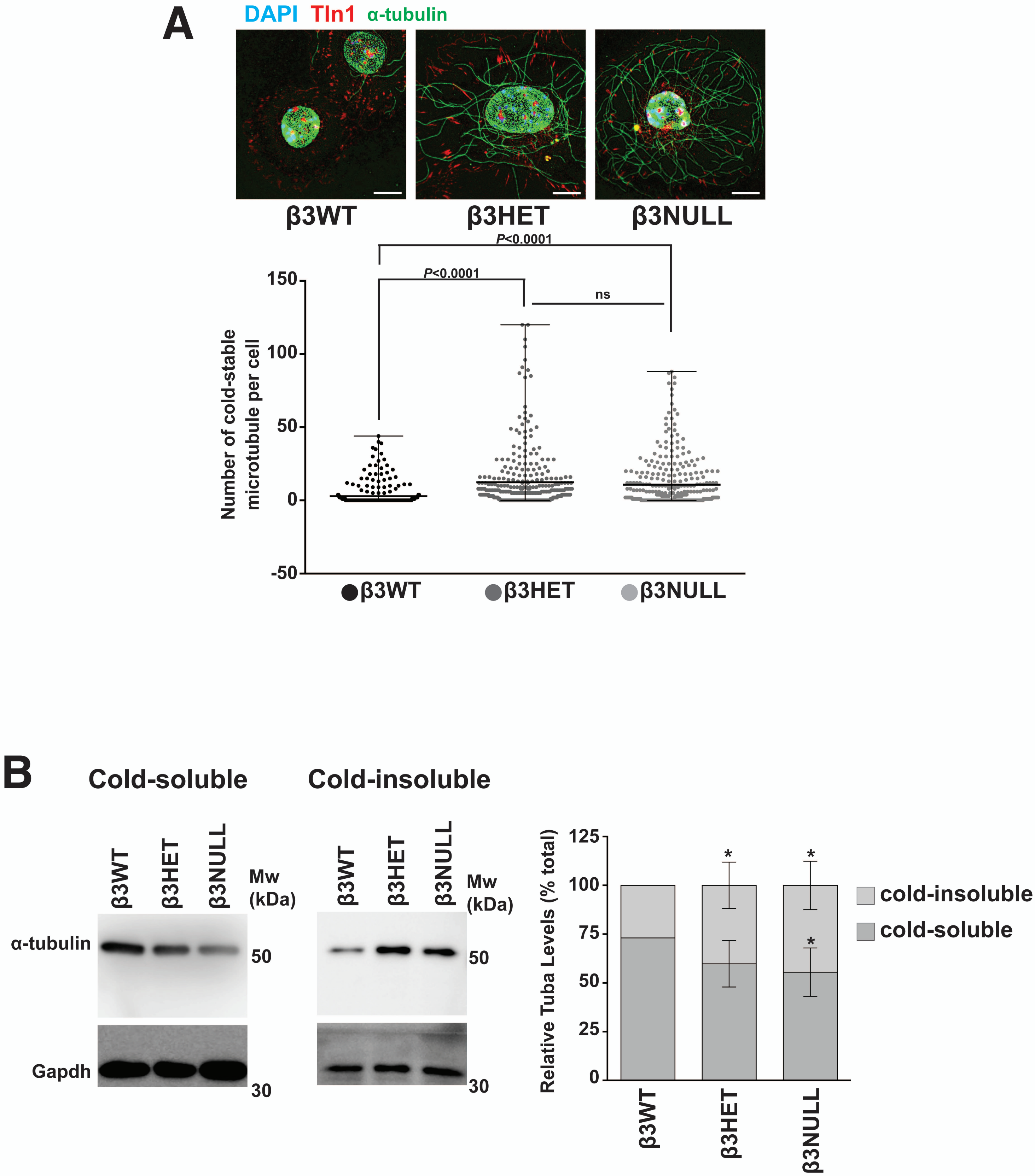
A
DAPI Tln1 α-tubulin
β3WT
β3HET
β3NULL
P<0.0001
P<0.0001
ns
Number of cold-stable microtubule per cell
150
100
50
0
-50
β3WT
β3HET
β3NULL
B
Cold-soluble
Cold-insoluble
β3WT
β3HET
β3NULL
Mw (kDa)
α-tubulin
50
Gapdh
30
Relative Tuba Levels (% total)
125
100
75
50
25
0
cold-insoluble
cold-soluble
*

Figure 5

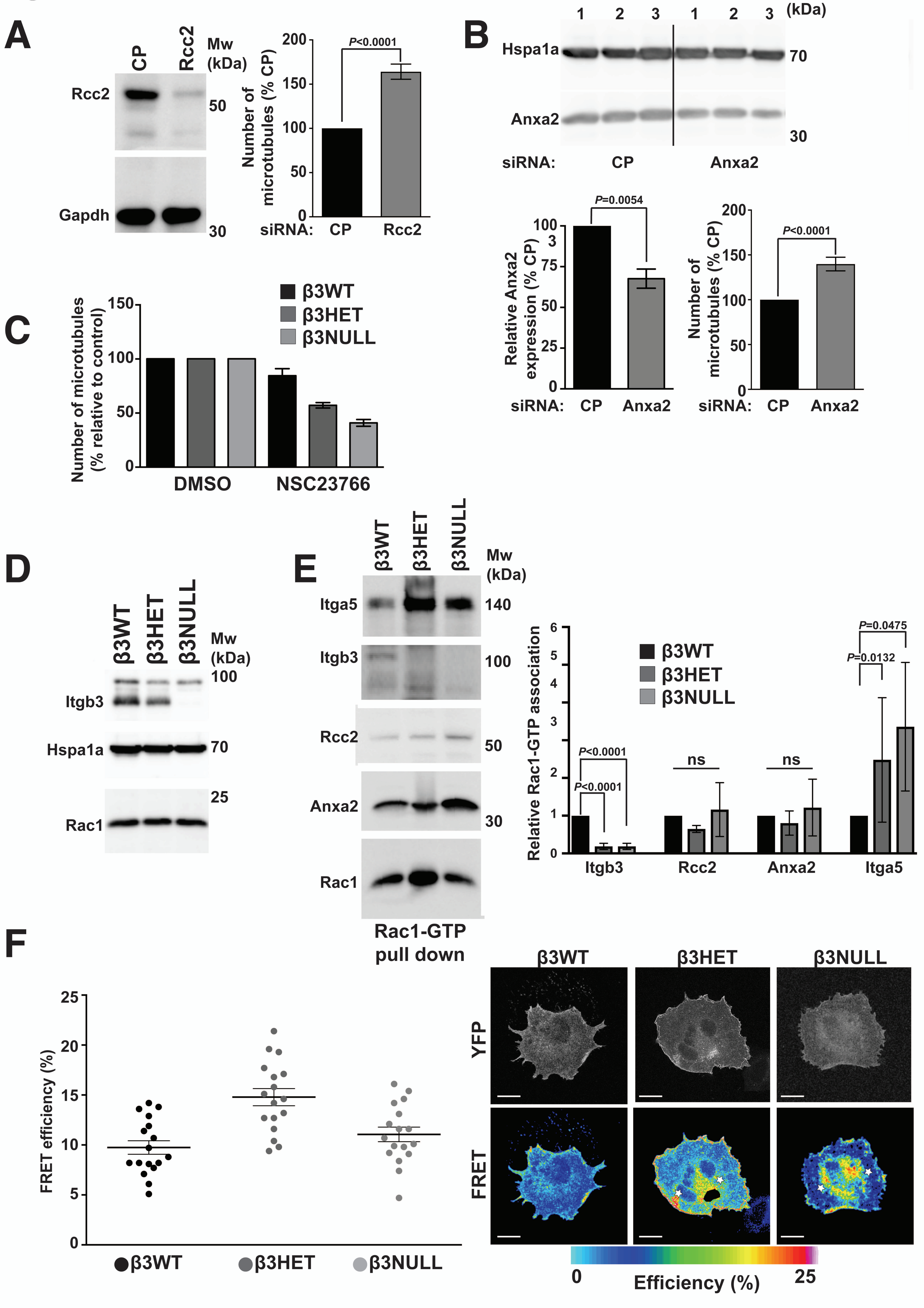

A
CP
Rcc2
Mw (kDa)
Rcc2
50
Gapdh
30
Number of microtubules (% CP)
P<0.0001
200
150
100
50
0
siRNA: CP Rcc2
B
1 2 3 1 2 3
Mw (kDa)
Hspa1a
70
Anxa2
30
siRNA: CP Anxa2
P=0.0054
Relative Anxa2 expression (% CP)
100
75
50
25
0
siRNA: CP Anxa2
P<0.0001
Number of microtubules (% CP)
200
150
100
50
0
siRNA: CP Anxa2
C
Number of microtubules (% relative to control)
150
100
50
0
β3WT
β3HET
β3NULL
DMSO
NSC23766
D
β3WT
β3HET
β3NULL
Mw (kDa)
100
Itgb3
Hspa1a
70
25
Rac1
E
β3WT
β3HET
β3NULL
Mw (kDa)
Itga5
140
Itgb3
100
Rcc2
50
Anxa2
30
Rac1
Rac1-GTP pull down
Relative Rac1-GTP association
6
5
4
3
2
1
0
β3WT
β3HET
β3NULL
P<0.0001
P<0.0001
ns
ns
P=0.0475
P=0.0132
Itgb3
Rcc2
Anxa2
Itga5
F
FRET efficiency (%)
25
20
15
10
5
0
β3WT
β3HET
β3NULL
β3WT
β3HET
β3NULL
YFP
FRET
0
Efficiency (%)
25

Figure EV1

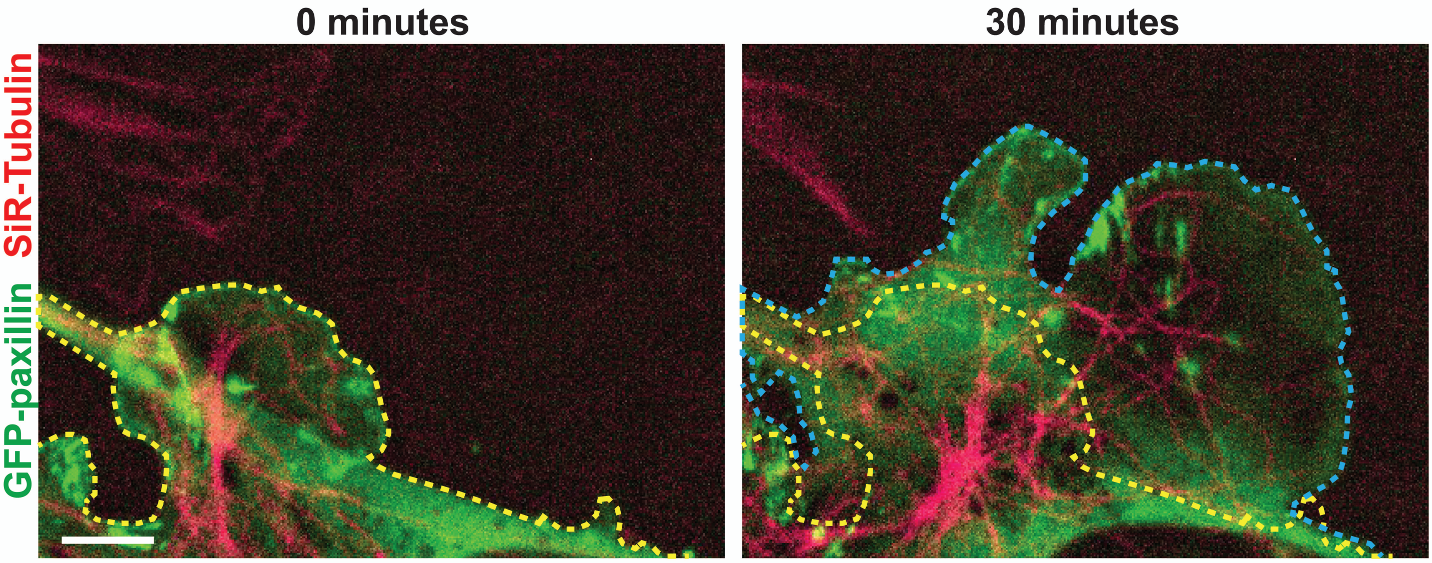

Figure EV2

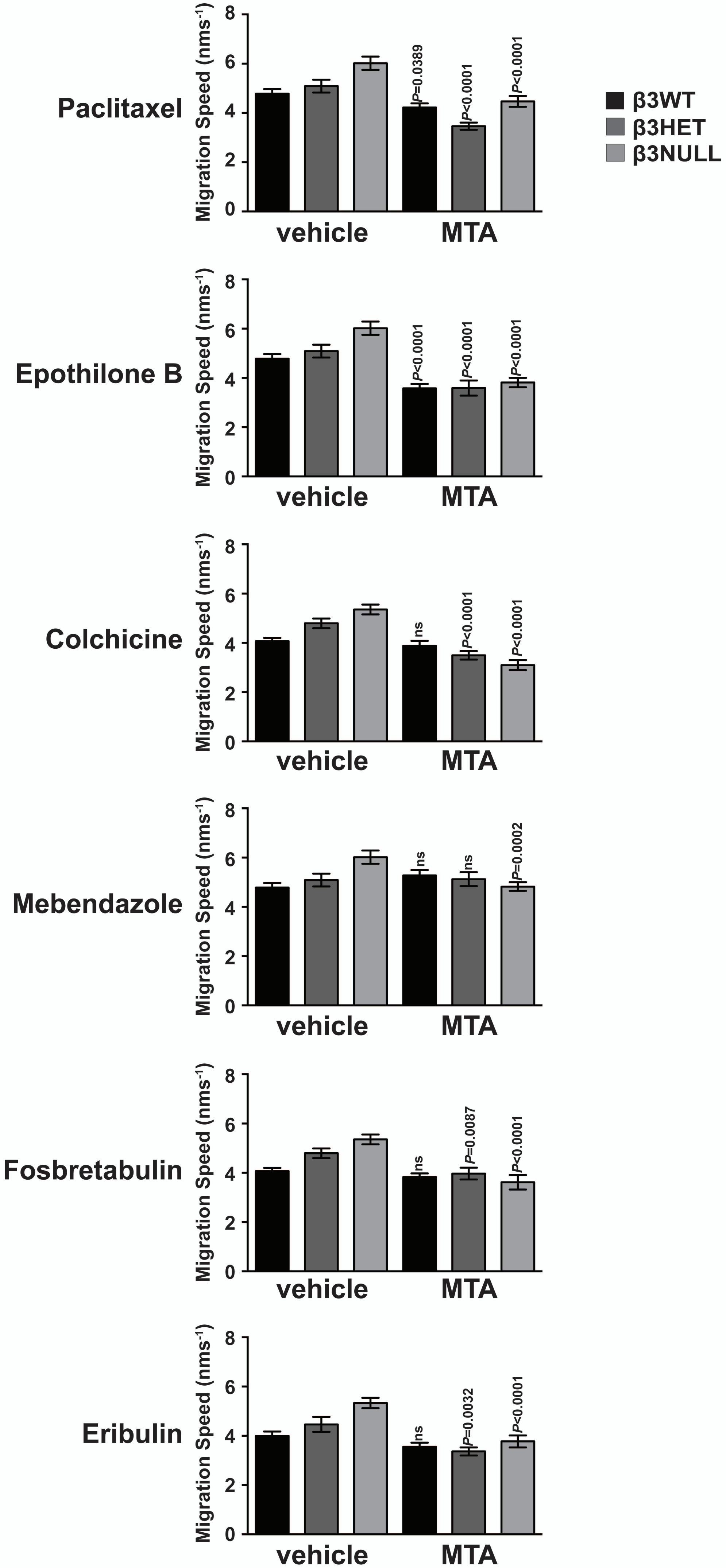

Paclitaxel
Epothilone B
Colchicine
Mebendazole
Fosbretabulin
Eribulin
Migration Speed (nms^{-1})
vehicle
MTA
β3WT
β3HET
β3NULL
P=0.0389
P<0.0001
P<0.0001
P<0.0001
P<0.0001
P<0.0001
ns
P<0.0001
P<0.0001
ns
ns
P=0.0002
ns
P=0.0087
P<0.0001
ns
P=0.0032
P<0.0001

Figure EV3

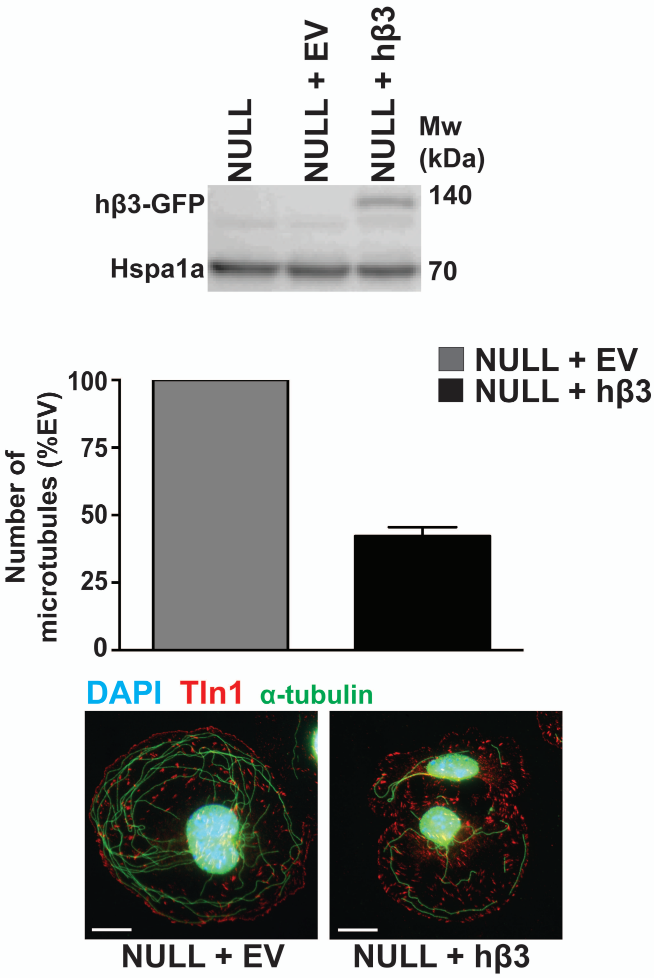
NULL
NULL + EV
NULL + hβ3
Mw
(kDa)
hβ3-GFP
140
Hspa1a
70
NULL + EV
NULL + hβ3
Number of
microtubules (%EV)
100
75
50
25
0
DAPI
Tln1
α-tubulin
NULL + EV
NULL + hβ3

Figure EV4

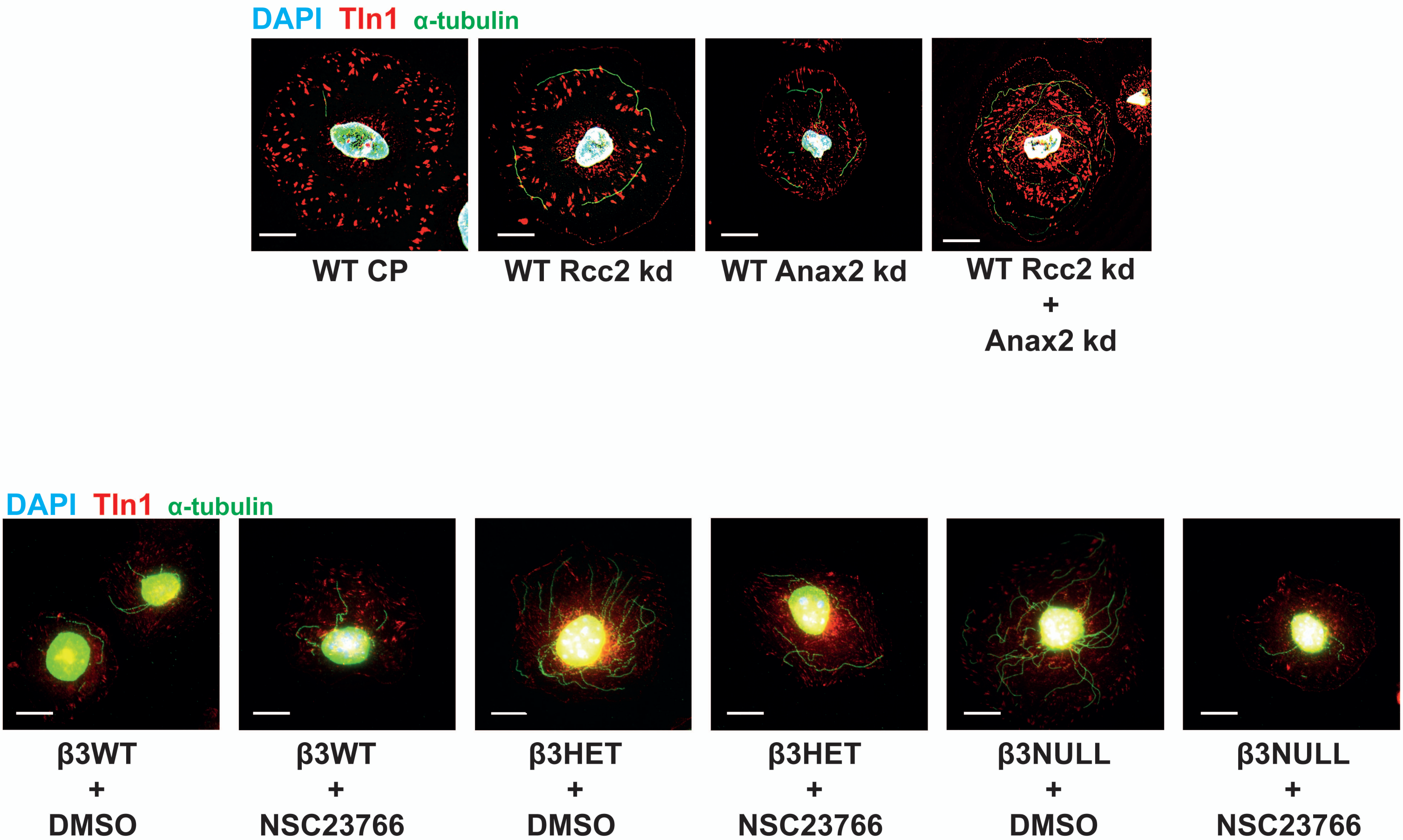
DAPI Tln1 α-tubulin
WT CP
WT Rcc2 kd
WT Anax2 kd
WT Rcc2 kd + Anax2 kd
DAPI Tln1 α-tubulin
β3WT + DMSO
β3WT + NSC23766
β3HET + DMSO
β3HET + NSC23766
β3NULL + DMSO
β3NULL + NSC23766

Figure EV5

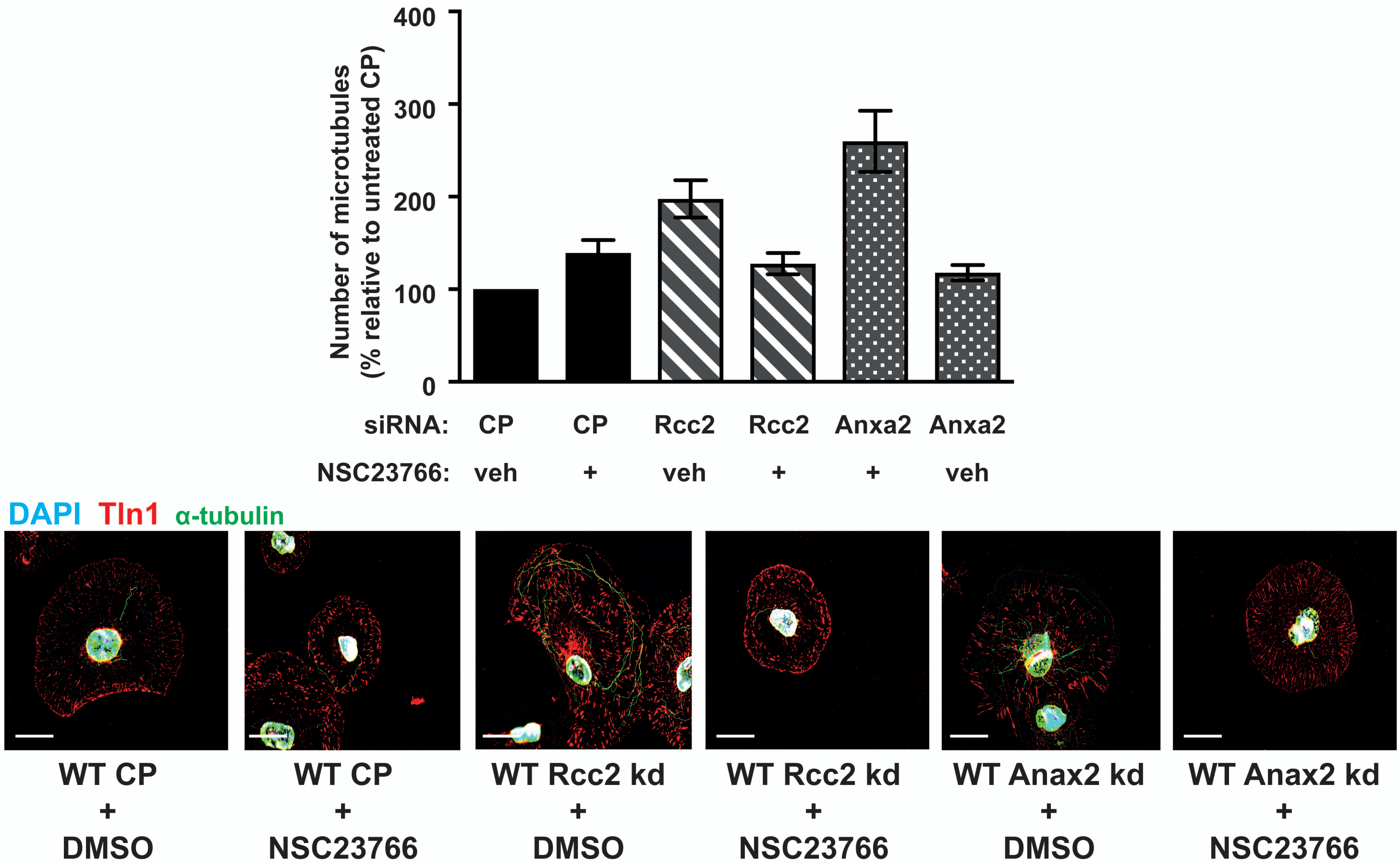

Number of microtubules (% relative to untreated CP)
400
300
200
100
0
siRNA: CP CP Rcc2 Rcc2 Anxa2 Anxa2
NSC23766: veh + veh + + veh
DAPI Tln1 α-tubulin
WT CP + DMSO
WT CP + NSC23766
WT Rcc2 kd + DMSO
WT Rcc2 kd + NSC23766
WT Anax2 kd + DMSO
WT Anax2 kd + NSC23766